J. Fluid Mech. (2001), *vol.* 430, *pp.* 381–400. Printed in the United Kingdom

A nonlinear evolution equation for pulsating Chapman–Jouguet detonations with chain-branching kinetics

By MARK SHORT

Theoretical and Applied Mechanics, University of Illinois, Urbana, IL 61801, USA

(Received 6 March 2000)

A nonlinear evolution equation for pulsating Chapman–Jouguet detonations with chain-branching kinetics is derived. We consider a model reaction system having two components: a thermally neutral chain-branching induction zone governed by an Arrhenius reaction, terminating at a location where conversion of fuel into chain radical occurs; and a longer exothermic main reaction layer or chain-recombination zone having a temperature-independent reaction rate. The evolution equation is derived under the assumptions of a large activation energy in the induction zone and a slow evolution time based on the particle transit time through the induction zone, and is autonomous and second-order in time in the shock velocity perturbation. It describes both stable and unstable solutions, the latter leading to stable periodic limit cycles, as the ratio of the length of the chain-recombination zone to chain-induction zone, the exothermicity of reaction, and the specific heats ratio are varied. These dynamics correspond remarkably well with numerical solutions conducted earlier for a model three-step chain-branching reaction.

1. Introduction

Unsteady one-dimensional detonation waves are known to undergo a pulsating form of instability (McVey & Toong 1971; Alpert & Toong 1972; Lehr 1972; Kaneshige & Shepherd 1996). An understanding of the intricate coupling between the exothermic reactive chemistry and nonlinear gasdynamic wave propagation which leads to the instability is highly desirable. However, a general analytical description of this nonlinear behaviour is a matter of severe mathematical complexity. Nevertheless, major advances can be made by exploiting limiting asymptotic forms of the problem, and the present work follows in this mould through the derivation of a nonlinear evolution equation for Chapman–Jouguet detonations with model chain-branching reaction kinetics.

To date, the majority of theoretical work on one-dimensional detonation stability has been conducted for Arrhenius one-step-reaction chemistry (Bourlioux, Majda & Roytburd 1991; Buckmaster & Ludford 1986; Buckmaster 1988; Short 1996, 1997; Yao & Stewart 1996). Two notable exceptions are those of Abouseif & Toong (1982) and Clavin & He (1996). Abouseif & Toong (1982) consider a two-zone detonation structure consisting of a high-activation-energy weak-heat-release induction zone followed by an exothermic main reaction layer of finite spatial extent. Although *ad-hoc*, the analysis does consider Chapman–Jouguet detonations, i.e. waves whose equilibrium flow is sonic in a frame attached to the lead detonation shock. This

isolates the main detonation structure from the equilibrium flow. Clavin & He (1996) also examine a similar two-zone detonation structure, but the analysis only applies in the limit of very high detonation overdrive. In reality, almost all detonations run at, or very close to, the Chapman–Jouguet velocity, and this situation of practical importance is the concern of the present paper.

In practice, a large class of chemical reactions is not represented effectively by a one-step Arrhenius reaction model. Rather, a large majority of chemical reactions are chain branching and proceed by a sequence of chain-initiation, chain-branching and chain-termination stages. The dynamics of a pulsating detonation wave for model chain-branching reaction kinetics have been previously studied by Short & Quirk (1997) and Short, Kapila & Quirk (1999). The three-step chain-branching model studied by these authors consists of thermally-neutral chain-initiation and chain-branching steps, both governed by Arrhenius kinetics, followed by a temperature-independent chain-termination step, where heat is released. Specifically, the reaction mechanism is,

$$\left.\begin{array}{ll} \text{Chain-initiation:} & F \rightarrow Y, \\ \text{Chain-branching:} & F + Y \rightarrow 2Y, \\ \text{Chain-termination:} & Y \rightarrow P, \end{array}\right\} \tag{1.1}$$

for fuel F, chain-radical Y and product P. Although elementary, the model mimics the essential dynamics of a chain-branching reaction. In Short & Quirk (1997) a stability analysis is performed with the chain-branching cross-over temperature T_B, i.e. the temperature at which chain-branching and chain-termination rates are equal, as the bifurcation parameter. In the steady structure, this parameter controls the ratio of the length of the temperature-sensitive chain-branching induction zone l_i to that of the temperature-insensitive chain-termination zone l_r. Stable detonations are predicted to occur when $l_i \ll l_r$, i.e. when the detonation structure is dominated by the chain-termination zone (typical of hydrogen–oxygen–diluent systems, e.g. Fickett, Jacobson & Schott 1972). For the parameter study performed in Short & Quirk (1997), as T_B is increased, i.e. the ratio l_i/l_r increases, the detonation undergoes a Hopf bifurcation leading to a nonlinear pulsating oscillation in the form a single-period, constant-amplitude, limit-cycle evolution. It is the dynamics of this transition from stable solutions to periodic, nonlinear behaviour that we aim to capture here by the derivation of an appropriate nonlinear evolution equation.

The present work follows in the spirit of Abouseif & Toong (1982), and uses a two-step chain-branching reaction model, a model extensively used at the Naval Research Laboratories for the purposes of large-scale computations (e.g. Oran & Boris 1986). The model has two components: a thermally neutral chain-branching induction zone and an exothermic main reaction layer or chain-recombination layer of finite extent. The extent of the induction zone is controlled by a reaction rate of Arrhenius form, but no heat is released due to reaction. This mimics the fact that chain-initiation and chain-branching reactions typically liberate only a small amount of heat. The end of the induction zone corresponds to the point where a rapid conversion of fuel into radical occurs (Short & Quirk 1997). The reaction rate in the exothermic chain-recombination layer is taken to be independent of temperature, typical of many chain-termination reactions, and such that the spatial extent of this layer is much greater than that of the induction zone. This is to mimic the detonation structure found in Short & Quirk (1997) for lower values of T_B, where stable detonations occur. Although this model falls short of full reaction kinetics, and indeed is not as complex as that studied in Short & Quirk (1997), it does, in contrast to the classical

one-step Arrhenius model, retain some of the essential chemical dynamics of a real chain-branching reaction.

To proceed we need to invoke two assumptions on the detonation structure and evolution dynamics. First, we assume a large activation energy in the induction zone kinetics, consistent with the induction zone behaviour in Short & Quirk (1997). Then we restrict ourselves to examining situations of low-frequency pulsating instabilities on evolution times that are slow on the time scale of the particle transit time through the smaller induction zone. This appears to be a highly reasonable approach since the numerical calculations in Short & Quirk (1997) appear to show that the evolution scales are slower even than the particle passage time through the much longer main reaction zone. This slowly evolving approach was first used by Buckmaster & Ludford (1986) and Buckmaster (1988) and later by Yao & Stewart (1996) in studying detonation dynamics for a one-step Arrhenius reaction in the limit of large activation energy.

The nonlinear evolution equation we derive here for Chapman–Jouguet detonations with our model two-stage chain-branching reaction mechanism has the second-order autonomous form

$$\alpha_0 h_{\tau\tau\tau} e^{\alpha_5 h_\tau} + h_{\tau\tau}[\alpha_1 + \alpha_2 e^{\alpha_5 h_\tau}] + \alpha_3 h_\tau + \alpha_4 h_{\tau\tau}^2 e^{\alpha_5 h_\tau} = 0,$$

where h_τ is the shock velocity perturbation $D_n \sim D + \epsilon h_\tau$, and α_i, $i = 1$ to 5, are constants determined by the analysis. Numerical solutions reveal that the evolution equation has stable solutions ($h_\tau = 0$) and unstable solutions leading to stable, periodic nonlinear limit-cycle oscillations.

2. Model

The propagation of the detonation is determined by the compressible reactive Euler equations for an ideal gas. Dimensionless equations for density, ρ, pressure, p, velocity u, temperature T and sound speed c can then be written in the conservative form

$$\left.\begin{aligned} \frac{\partial}{\partial n}[\rho u] &= -\frac{\partial \rho}{\partial t}, \\ \frac{\partial}{\partial n}[p + \rho u^2] &= -\frac{\partial}{\partial t}[\rho u], \\ \frac{\partial}{\partial n}\left[\frac{\gamma p}{(\gamma-1)\rho} + \frac{u^2}{2} - \beta\lambda\right] &= -\frac{\partial u}{\partial t} - \frac{1}{u}\left[\frac{1}{(\gamma-1)\rho}\frac{\partial p}{\partial t} - \frac{\gamma p}{(\gamma-1)\rho^2}\frac{\partial \rho}{\partial t} - \beta\frac{\partial \lambda}{\partial t}\right], \end{aligned}\right\} \tag{2.1}$$

assuming an ideal equation of state,

$$c^2 = T = \frac{\gamma p}{\rho}. \tag{2.2}$$

Here β is the heat release scaled with respect to the post-shock thermal energy (Short & Stewart 1999), γ the ratio of specific heats and λ corresponds to the reaction progress variable in either the induction zone or main reaction layer, satisfying the consumption equation

$$\frac{\partial \lambda}{\partial n} = \frac{1}{u}\left[r - \frac{\partial \lambda}{\partial t}\right], \tag{2.3}$$

for corresponding reaction rate r. Non-dimensional variables are determined by the scales

$$\rho = \frac{\tilde{\rho}}{\tilde{\rho}_s}, \qquad p = \frac{\tilde{p}}{\tilde{\rho}_s \tilde{c}_s^2}, \qquad u = \frac{\tilde{u}}{\tilde{c}_s}, \qquad T = \frac{\tilde{T}}{\tilde{T}_s}, \qquad c = \frac{\tilde{c}}{\tilde{c}_s}, \tag{2.4}$$

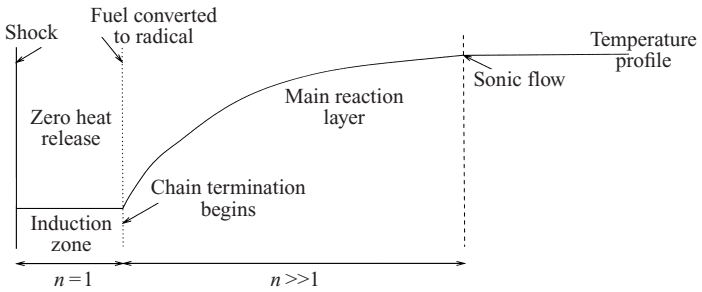

FIGURE 1. A schematic of the steady detonation structure for the two-step chain-branching reaction model.

while length and time are scaled according to

$$n = \frac{\tilde{n}}{\tilde{n}_s}, \qquad t = \frac{\tilde{t}}{\tilde{n}_s/\tilde{c}_s}. \tag{2.5}$$

The subscript s refers to the immediate post-shock values in the steady wave, while $\tilde{n}_s$ is chosen so that $n = 1$ corresponds to the end of the induction zone in the steady wave (see below).

Under these scalings, the steady shock conditions are given by

$$\rho = 1, \qquad p = \frac{1}{\gamma}, \qquad u = M_s, \qquad T = 1, \tag{2.6}$$

where M_s is the steady post-shock flow Mach number.

3. Detonation structure

The detonation structure is determined by specification of reaction rates. As mentioned previously, we employ a two-step chain-branching reaction model having two components: a thermally neutral chain-branching induction zone and an exothermic main reaction layer or chain-recombination layer of finite extent, as shown in figure 1.

3.1. *Induction zone reaction rate*

The dynamics in the induction zone are controlled by a reaction rate of Arrhenius form in which no heat is released due to reaction. This mimics the fact that chain-initiation and chain-branching reactions typically liberate only a small amount of heat. Therefore, in the induction zone we set $\beta = 0$, and

$$r = M_s \exp\left[\frac{1}{\epsilon}\left(1 - \frac{1}{T}\right)\right], \tag{3.1}$$

where ϵ is the inverse activation energy, assumed small, so that

$$\epsilon \ll 1. \tag{3.2}$$

At the shock $\lambda = 0$, while the termination of the induction zone is signalled when $\lambda = 1$, where fuel is instantaneously converted into chain-radical.

3.2. *Main heat release layer reaction rate*

The reaction rate in the exothermic chain-recombination (termination) layer is assumed to be independent of the local thermodynamic state, a good model for chain-

termination reactions. The rate is taken such that the spatial extent of this layer is much greater than that of the induction zone, to mimic the detonation structure found in Short & Quirk (1997) for lower values of T_B, as described previously. In the main heat release layer, we therefore assume a reaction rate of the well-known form

$$r = k(1-\lambda)^{1/2} \tag{3.3}$$

where k is the rate constant, taking $k \ll 1$ to ensure that the main heat release layer is much longer than the induction zone. The fractional power used in (3.3) is to represent the fact that several elementary reaction steps are usually involved in determining the overall recombination mechanism (Buckmaster & Ludford 1982). It also has the advantage that the main heat release layer has finite extent. It should be noted, however, that many other forms of reaction rate could be considered with equal ease. Also, $\lambda = 0$ marks the start of the main heat release layer, beyond which chain recombination occurs and heat is released, as in the reaction model of Short & Quirk (1997), while $\lambda = 1$ signals the rear equilibrium point of the detonation, where sonic flow conditions apply since the detonation is running at Chapman–Jouguet speed.

4. Derivation of the nonlinear evolution equation

Let the shock front follow the path $n = h(t)$. We seek those solutions having slowing evolving dynamics, specifically one which is $O(1/\epsilon)$ on the scale of the particle transit time through the induction zone. Introducing the slow time variable

$$\tau = \epsilon t \tag{4.1}$$

and transforming to a shock-attached coordinate system, the system (2.1) becomes,

$$\left.\begin{aligned}
&\frac{\partial}{\partial n}[\rho(u-\epsilon h_\tau)] = -\epsilon\frac{\partial \rho}{\partial \tau},\\
&\frac{\partial}{\partial n}[p+\rho u(u-\epsilon h_\tau)] = -\epsilon\frac{\partial}{\partial \tau}[\rho u],\\
&\frac{\partial}{\partial n}\left[\frac{\gamma p}{(\gamma-1)\rho}+\frac{(u-\epsilon h_\tau)^2}{2}-\beta\lambda\right] = -\epsilon\frac{\partial u}{\partial \tau}-\frac{\epsilon}{(u-h_\tau)}\\
&\qquad\qquad\times\left[\frac{1}{(\gamma-1)\rho}\frac{\partial p}{\partial \tau}-\frac{\gamma p}{(\gamma-1)\rho^2}\frac{\partial \rho}{\partial \tau}-\beta\frac{\partial \lambda}{\partial \tau}\right],\\
&\frac{\partial \lambda}{\partial n} = \frac{1}{(u-\epsilon h_\tau)}\left[r-\epsilon\frac{\partial \lambda}{\partial \tau}\right],
\end{aligned}\right\} \tag{4.2}$$

where $n = 0$ now represents the shock position in the time-varying frame. Correspondingly, the detonation Mach number D_n has the expansion

$$D_n \sim D + \epsilon h_\tau, \tag{4.3}$$

where D is the Chapman–Jouguet detonation Mach number in the unperturbed wave.

4.1. *Induction zone analysis*

There is no heat release in the induction zone, implying $\beta = 0$, while the kinetics are governed by the reaction rate (3.1), with $\epsilon \ll 1$. To $O(\epsilon)$, appropriate expansions in

this zone are

$$\rho = 1 + \epsilon\rho^{(1)}, \quad p = \frac{1}{\gamma} + \epsilon p^{(1)}, \quad u = M_s + \epsilon u^{(1)}, \quad T \sim 1 + \epsilon T^{(1)}, \tag{4.4}$$

with corresponding $O(\epsilon)$ shock conditions,

$$u^{(1)} = k_u h_\tau, \quad p^{(1)} = k_p h_\tau, \quad T^{(1)} = k_T h_\tau, \quad \rho^{(1)} = k_\rho h_\tau, \quad \lambda = 0. \tag{4.5}$$

The coefficients appearing in (4.5) are given in the Appendix. To $O(\epsilon)$, it can be shown that the perturbations satisfy the quasi-steady reduced equations,

$$\frac{\partial}{\partial n}[\rho u] = 0, \quad \frac{\partial}{\partial n}[p + \rho u^2] = 0, \quad \frac{\partial}{\partial n}\left[\frac{\gamma p}{(\gamma - 1)\rho} + \frac{u^2}{2}\right] = 0. \tag{4.6}$$

Substituting (4.4) into (4.6) gives the solution

$$u^{(1)} = k_u h_\tau, \quad p^{(1)} = k_p h_\tau, \quad T^{(1)} = k_T h_\tau, \quad \rho^{(1)} = k_\rho h_\tau, \tag{4.7}$$

so that the perturbations at the shock are propagated along particle paths without change of form (since $\beta = 0$).

The end of the induction zone, which marks the point at which fuel is converted into chain radical, is determined by considering the reaction rate (3.1), which, with expansions (4.4), becomes

$$\frac{\partial \lambda}{\partial n} = \mathrm{e}^{T^{(1)}} \quad \text{or} \quad \frac{\partial \lambda}{\partial n} = \mathrm{e}^{k_T h_\tau}. \tag{4.8}$$

Its solution, having $\lambda = 0$ at $n = 0$, is given by

$$\lambda = n\mathrm{e}^{k_T h_\tau}. \tag{4.9}$$

Under the assumptions of our two-step chain-branching model, the end of the induction zone is then located at $\lambda = 1$, where

$$n = F(\tau) = \mathrm{e}^{-k_T h_\tau}. \tag{4.10}$$

Thus $O(\epsilon)$ perturbations to the detonation shock lead to $O(1)$ changes in the location of the fuel to chain-radical conversion front due to the exponential sensitivity of the Arrhenius reaction rate, a finding first observed by Buckmaster & Ludford (1986).

4.2. *Main heat release layer analysis*

The end of the induction zone corresponds to the point where fuel is converted into chain radical, but also marks the start of the main reaction, or chain-recombination, layer where heat is released as chain radical is converted into product. The analysis of this layer begins by making the transformation

$$m = n - F(\tau) \tag{4.11}$$

so $m = 0$ marks the point where λ, now defined as the progress variable for the chain-termination reaction, is zero. In this main reaction layer the reaction rate is given by (3.3), independent of temperature, corresponding to the dynamics of chain-termination reactions suggested in Short & Quirk (1997). Under the assumptions of our model, the length of the main reaction layer is made greater than the length of the induction zone through the choice

$$k = O(\epsilon\tilde{k}/\bar{\omega}) \ll 1 \tag{4.12}$$

for the rate constant k, with $\tilde{k} = O(1) > 0$. For the present we seek dynamics where $\bar{\omega}$ can take any appropriate scale such that $1 \gg \bar{\omega} \gg \epsilon$. Consequently, the evolution will be also slowly varying relative to the transit time of a particle through the steady (but longer) chain-termination region. The constant k is absorbed into the spatial variable m by the transformation

$$\tilde{m} = \frac{\epsilon}{\omega} m \tag{4.13}$$

where $\omega = \bar{\omega}/\tilde{k}$. To proceed with the analysis in the main reaction layer, it is convenient to transform from the spatial variable $\tilde{m}$ to the reaction progress variable λ as independent variable, a process facilitated by the relations

$$\left(\frac{\partial}{\partial t}\right)_{\tilde{m}} = \left(\frac{\partial}{\partial t}\right)_{\lambda} + \left(\frac{\partial \lambda}{\partial t}\right)_{\tilde{m}} \left(\frac{\partial}{\partial \lambda}\right), \qquad \left(\frac{\partial}{\partial \tilde{m}}\right)_{t} = \left(\frac{\partial \lambda}{\partial \tilde{m}}\right)_{t} \left(\frac{\partial}{\partial \lambda}\right). \tag{4.14}$$

It can also be shown that, to the order of analysis we will be concerned with, the relevant equations are given by

$$\left.\begin{aligned} \frac{\partial}{\partial \lambda}[\rho(u - \epsilon(h+F)_\tau)] &= -\omega \frac{u}{r} \frac{\partial \rho}{\partial \tau}, \\ \frac{\partial}{\partial \lambda}[p + \rho u(u - \epsilon(h+F)_\tau)] &= -\omega \frac{u}{r} \frac{\partial}{\partial \tau}[\rho u], \\ \frac{\partial}{\partial \lambda}\left[\frac{\gamma p}{(\gamma-1)\rho} + \frac{(u - \epsilon(h+F)_\tau)^2}{2} - \beta\lambda\right] &= -\omega \frac{u}{r} \frac{\partial u}{\partial \tau} - \frac{\omega}{r} \\ &\quad \times \left[\frac{1}{(\gamma-1)\rho} \frac{\partial p}{\partial \tau} - \frac{\gamma p}{(\gamma-1)\rho^2} \frac{\partial \rho}{\partial \tau} - \beta \frac{\partial \lambda}{\partial \tau}\right]. \end{aligned}\right\} \tag{4.15}$$

We now seek expansions in the main reaction layer of the form,

$$\left.\begin{aligned} \rho \sim \rho^{(0)} + \epsilon\rho^{(1)} + \omega\epsilon\rho^{(2)}, \quad p \sim p^{(0)} + \epsilon p^{(1)} + \omega\epsilon p^{(2)}, \\ u \sim u^{(0)} + \epsilon u^{(1)} + \omega\epsilon u^{(2)}, \quad \lambda \sim \lambda^{(0)} + \epsilon\lambda^{(1)}. \end{aligned}\right\} \tag{4.16}$$

The conditions for the $O(1)$ state at $\lambda = 0$ are the steady shock conditions (2.6), those for the $O(\epsilon)$ perturbations at $\lambda = 0$, (4.7), while the $O(\epsilon\omega)$ perturbations are all zero at $\lambda = 0$, since there are no corresponding $O(\epsilon\omega)$ terms in the induction zone.

The leading-order problem is simply the steady structure

$$\left.\begin{aligned} \frac{\partial}{\partial \lambda}[\rho^{(0)} u^{(0)}] = 0, \quad \frac{\partial}{\partial \lambda}[p^{(0)} + \rho^{(0)}[u^{(0)}]^2] = 0, \\ \frac{\partial}{\partial \lambda}\left[\frac{\gamma p^{(0)}}{(\gamma-1)\rho^{(0)}} + \frac{[u^{(0)}]^2}{2} - \beta\lambda\right] = 0, \end{aligned}\right\} \tag{4.17}$$

having as its solution the standard Rankine–Hugoniot relations for a Chapman–Jouguet detonation velocity

$$p^{(0)} = a + (\gamma^{-1} - a)(1 - \lambda)^{1/2}, \quad u^{(0)} = \frac{(1 - \gamma p^{(0)})}{\gamma M_s} + M_s, \quad \rho^{(0)} = \frac{M_s}{u^{(0)}}, \tag{4.18}$$

where

$$M_s^2 = \frac{2+(\gamma-1)D^2}{2\gamma D^2-(\gamma-1)}, \qquad a = \frac{\gamma^{-1}(1+\gamma D^2)}{2\gamma D^2+1-\gamma}. \tag{4.19}$$

An expression for the Chapman–Jouguet velocity D in terms of the pre-shock thermal-energy scaled heat release Q (Short & Stewart 1999) is given in the Appendix. Of particular interest to us is the sonic parameter given by

$$\eta = [u^{(0)}]^2 - \frac{\gamma p^{(0)}}{\rho^{(0)}} = \frac{(\gamma+1)(D^2-1)\zeta(\zeta(D^2-1)-(\gamma D^2+1)}{(2\gamma D^2+1-\gamma)(2+\gamma(D^2-1))}, \tag{4.20}$$

where

$$\zeta = (1-\lambda)^{1/2}. \tag{4.21}$$

It is easily seen that $\eta \to 0$ as $\zeta \to 0$, i.e. the flow is sonic at the point where reaction terminates.

Furthermore, equations (4.15) can be integrated directly subject to the conditions at $\lambda = 0$ mentioned previously. Using (4.16), the $O(\epsilon)$ first and $O(\epsilon\omega)$ second order problems may then be written in the combined form,

$$\boldsymbol{A}(\lambda)\cdot(\boldsymbol{y}^{(1)}(\lambda)+\omega\boldsymbol{y}^{(2)}(\lambda)) = \boldsymbol{C}_0(\lambda)h_\tau + \boldsymbol{C}_1(\lambda)F_\tau + \omega\boldsymbol{C}_2(\lambda), \tag{4.22}$$

where $\boldsymbol{y} = [\rho, u, p]^T$,

$$\boldsymbol{A} = \begin{bmatrix} u^{(0)} & \rho^{(0)} & 0 \\ [u^{(0)}]^2 & 2u^{(0)}\rho^{(0)} & 1 \\ -\dfrac{\gamma p^{(0)}}{(\gamma-1)[\rho^{(0)}]^2} & u^{(0)} & \dfrac{\gamma}{(\gamma-1)\rho^{(0)}} \end{bmatrix}, \tag{4.23}$$

$$\boldsymbol{C}_0 = \begin{bmatrix} \rho^{(0)} + M_s k_\rho + k_u - 1 \\ 0 \\ u^{(0)} + \dfrac{1}{(\gamma-1)}(\gamma k_p - k_\rho) + M_s(k_u-1) \end{bmatrix}, \tag{4.24}$$

and

$$\boldsymbol{C}_1 = \begin{bmatrix} \rho^{(0)} - 1 \\ 0 \\ u^{(0)} - M_s \end{bmatrix}, \quad \boldsymbol{C}_2 = \begin{bmatrix} N_1 \\ N_2 \\ N_3 \end{bmatrix}. \tag{4.25}$$

The terms N_1, N_2 and N_3 are given by

$$\left.\begin{aligned} N_1 &= -\int_0^\lambda \frac{u^{(0)}}{r^{(0)}}\frac{\partial\rho^{(1)}}{\partial\tau}\,\mathrm{d}\lambda, \\ N_2 &= -\int_0^\lambda \frac{u^{(0)}}{r^{(0)}}\left[u^{(0)}\frac{\partial\rho^{(1)}}{\partial\tau} + \rho^{(0)}\frac{\partial u^{(1)}}{\partial\tau}\right]\mathrm{d}\lambda, \\ N_3 &= -\int_0^\lambda \frac{u^{(0)}}{r^{(0)}}\frac{\partial u^{(1)}}{\partial\tau} + \frac{1}{r^{(0)}}\left[\frac{1}{(\gamma-1)\rho^{(0)}}\frac{\partial p^{(1)}}{\partial\tau} - \frac{\gamma}{(\gamma-1)}\frac{p^{(0)}}{[\rho^{(0)}]^2}\frac{\partial\rho^{(1)}}{\partial\tau} - \beta\frac{\partial\lambda^{(1)}}{\partial\tau}\right]\mathrm{d}\lambda, \end{aligned}\right\} \tag{4.26}$$

and result from the inclusion of time-derivative terms appearing on the right-hand

side of (4.15), which account for first-order slowly varying acoustic effects in the main reaction layer. To calculate the perturbation solutions $\boldsymbol{y}^{(1)}$ and $\boldsymbol{y}^{(2)}$ we need the inverse of $\boldsymbol{A}$, given by

$$\boldsymbol{A}^{-1} = \frac{\mathrm{adj}(\boldsymbol{A})}{\det(\boldsymbol{A})} = \frac{(\gamma-1)}{\eta} \times \begin{bmatrix} u^{(0)}\dfrac{(\gamma+1)}{(\gamma-1)} & -\dfrac{\gamma}{(\gamma-1)} & \rho^{(0)} \\ -\dfrac{\gamma([u^{(0)}]^2 + p^{(0)}/\rho^{(0)})}{(\gamma-1)\rho^{(0)}} & \dfrac{u^{(0)}\gamma}{(\gamma-1)\rho^{(0)}} & -u^{(0)} \\ u^{(0)}\left([u^{(0)}]^2 + \dfrac{2\gamma}{(\gamma-1)}\dfrac{p^{(0)}}{\rho^{(0)}}\right) & -\left([u^{(0)}]^2 + \dfrac{\gamma}{(\gamma-1)}\dfrac{p^{(0)}}{\rho^{(0)}}\right) & [u^{(0)}]^2\rho^{(0)} \end{bmatrix}, \tag{4.27}$$

which is singular as $\eta \to 0$.

Restricting our attention first to the $O(\epsilon)$ perturbation problem, we can solve the system (4.22) to find

$$\left.\begin{aligned} \rho^{(1)} &= \frac{(\gamma-1)}{\eta}[A_1 h_\tau + A_2 F_\tau] + B_1(\lambda)h_\tau + B_2(\lambda)F_\tau, \\ u^{(1)} &= \frac{(\gamma-1)}{\eta}\left[-\left(\frac{u^{(0)}}{\rho^{(0)}}\right)_{\lambda=1}[A_1 h_\tau + A_2 F_\tau]\right] + B_3(\lambda)h_\tau + B_4(\lambda)F_\tau, \\ p^{(1)} &= \frac{(\gamma-1)}{\eta}[([u^{(0)}]^2)_{\lambda=1}[A_1 h_\tau + A_2 F_\tau]] + B_5(\lambda)h_\tau + B_6(\lambda)F_\tau, \end{aligned}\right\} \tag{4.28}$$

where A_1, A_2 (constants), B_i, $i = 1,6$ (functions of λ) are given in the Appendix. All solutions are singular at the Chapman–Jouguet sonic point $\eta = 0$, unless the compatibility condition

$$A_1 h_\tau + A_2 F_\tau = 0 \quad \text{or} \quad A_1 h_\tau - k_T A_2 h_{\tau\tau} \mathrm{e}^{-k_T h_\tau} = 0 \tag{4.29}$$

is satisfied. Equation (4.29) is an evolution equation governing the $O(\epsilon)$ dynamics of the front. Seeking normal mode solutions of the form $h_\tau \propto \exp(\delta t)$ for the linearized equation (4.29), leads to the eigenvalue condition

$$\delta = \frac{A_1}{k_T A_2}. \tag{4.30}$$

It is easily shown from the relations in the Appendix, that $A_1 > 0$, $A_2 < 0$ and $k_T < 0$ for all D and γ, so that to the order of the analysis we have considered thus far, (4.30) represents a positive real eigenvalue. This is precisely the situation found in Buckmaster & Ludford (1986) for their high-activation-energy, one-step Arrhenius kinetic model, so apparently there is no qualitative difference thus far in considering a spatial distributed main heat release layer, rather than a jump discontinuity. Numerical calculations in Short & Quirk (1997), however, reveal that in practice the detonation first becomes unstable to a pair of complex eigenvalues that undergo a Hopf bifurcation.

The conclusion we are drawn to, therefore, is that it seems unreasonable, at first, to assume that the evolution is quasi-steady on the time scale associated with particle passage through the longer chain-termination region. One strategy to correct this

deficiency would be to make the rate constant k of size $O(\epsilon)$, so that $\bar{\omega} = O(1)$, where the time-derivative terms in (4.15) become $O(1)$ rather than $O(\omega)$. However, it turns out that the resulting problem has no explicit analytical solution. A second strategy is to recognize that Short & Quirk (1997) have shown that the evolution time scales of pulsating detonations do appear to be slow, with typical periods in the region of 30 to 40 times longer than the time scale of particle passage through the chain-termination zone. It seems appropriate, therefore, to attempt a formal asymptotic solution to the problem by the strategy of Picard iteration, using $\bar{\omega}$ ($\epsilon \ll \bar{\omega} \ll 1$) as the iteration or control parameter. In order to obtain a solution in this manner, we proceed by evaluating the $O(\epsilon\omega)$ problem as determined by (4.22), set $\bar{\omega} = 1$ and compare the predictions of the resulting evolution equation with those obtained numerically by Short & Quirk (1997). This asymptotic strategy is equivalent to retaining first-order acoustic effects in the main heat release layer.

First, we recognize that the regular part of the first-order perturbations (4.28) can be written as

$$\rho^{(1)} = B_1 h_\tau + B_2 F_\tau, \quad u^{(1)} = B_3 h_\tau + B_4 F_\tau, \quad p^{(1)} = B_5 h_\tau + B_6 F_\tau. \tag{4.31}$$

To calculate the $O(\epsilon\omega)$ terms governed by (4.22), we need an expression for $\lambda^{(1)}(\tilde{m})$ in terms of λ. It can be shown from (2.3), (3.3) and (4.16) that the relevant equation is

$$\frac{\partial \lambda^{(1)}}{\partial \lambda} + \frac{\lambda^{(1)}}{2(1-\lambda)} = -\frac{(u^{(1)} - h - F_\tau)}{u^{(0)}} \tag{4.32}$$

with solution satisfying $\lambda^{(1)} = 0$ when $\lambda = 0$

$$\lambda^{(1)} = -(1-\lambda)^{1/2} \int_0^\lambda \frac{(u^{(1)} - h_\tau - F_\tau)}{u^{(0)}(1-\lambda)^{1/2}}\, \mathrm{d}\lambda. \tag{4.33}$$

Note that the integration in (4.33) and those for the integrals I_1 to I_6 appearing below are facilitated by the identity,

$$\int_0^\lambda \frac{\mathrm{d}\lambda}{\sqrt{1-\lambda}} = -2 \int_1^\zeta \mathrm{d}\zeta. \tag{4.34}$$

The solution for $\lambda^{(1)}$ can then be written as

$$\lambda^{(1)} = B_7(\lambda) h_\tau + B_8(\lambda) F_\tau, \tag{4.35}$$

with B_7 and B_8 given in the Appendix.

With the $O(\epsilon)$ solution now known, the system (4.22) may be inverted to determine the $O(\epsilon\omega)$ solution, which is again singular as $\eta \to 0$, $\lambda \to 0$. In particular, as $\eta \to 0$, the solution for $\rho^{(1)} + \omega\rho^{(2)}$ has the asymptotic form

$$\rho^{(1)} + \omega\rho^{(2)} \to \frac{(\gamma-1)}{\eta}\left[A_1 h_\tau + A_2 F_\tau + \omega\left\{\left(u^{(0)}\frac{(\gamma+1)}{(\gamma-1)} I_1 - \frac{\gamma}{(\gamma-1)} I_3 + \rho^{(0)} I_5\right)_{\lambda=1} h_{\tau\tau} + \left(u^{(0)}\frac{(\gamma+1)}{(\gamma-1)} I_2 - \frac{\gamma}{(\gamma-1)} I_4 + \rho^{(0)} I_6\right)_{\lambda=1} F_{\tau\tau}\right\}\right]. \tag{4.36}$$

The integral quantities I_1 to I_6 are defined in the Appendix. Singular solutions are eliminated by setting the quantity in the square brackets to zero. This leads to a new evolution equation for the shock front, which may be written in the form

$$\alpha_0 \tilde{k}^{-1} h_{\tau\tau\tau} \mathrm{e}^{-k_T h_\tau} + h_{\tau\tau}[\tilde{k}^{-1}\alpha_1 + \alpha_2 \mathrm{e}^{-k_T h_\tau}] + \alpha_3 h_\tau + \alpha_4 \tilde{k}^{-1} h_{\tau\tau}^2 e^{-k_T h_\tau} = 0, \tag{4.37}$$

after setting $\bar{\omega} = 1$, where

$$\left.\begin{aligned} \alpha_0 &= -k_T \left[u^{(0)} \frac{(\gamma+1)}{(\gamma-1)} I_2 - \frac{\gamma}{(\gamma-1)} I_4 + \rho^{(0)} I_6 \right]_{\lambda=1}, \\ \alpha_1 &= \left[u^{(0)} \frac{(\gamma+1)}{(\gamma-1)} I_1 - \frac{\gamma}{(\gamma-1)} I_3 + \rho^{(0)} I_5 \right]_{\lambda=1}, \\ \alpha_2 &= -A_2 k_T, \quad \alpha_3 = A_1, \quad \alpha_4 = -k_T \alpha_0. \end{aligned}\right\} \tag{4.38}$$

Equation (4.37) is an automonous second-order equation in the shock velocity perturbation which has $h_\tau = 0$ and $h_{\tau\tau} = 0$ as the only equilibrium point. Although derived for $\bar{\omega} \ll 1$, we expect (4.37) to be a model equation which captures the essential dynamics involved when $\bar{\omega} = 1$. Depending on the coefficients $\tilde{k}$, α_1 to α_4 and k_T, the equation could describe stable or unstable solutions near the equilibrium point, and possess stable or unstable periodic solutions when the equilibrium point is unstable. For the parameter space we are concerned with, namely $1.2 \leqslant \gamma \leqslant 1.6$ and $1 \leqslant Q \leqslant 8$, it can be shown numerically that $\alpha_0 > 0$, $\alpha_1 > 0$, $\alpha_2 < 0$, $\alpha_3 > 0$ and $\alpha_4 > 0$. Ignoring the exponential terms in (4.37), the underlying dynamics of the evolution equation is that of a linear oscillator with a nonlinear damping term that limits the growth of linearly unstable solutions. The linear equation

$$\alpha_0 \tilde{k}^{-1} h_{\tau\tau\tau} + h_{\tau\tau} [\tilde{k}^{-1} \alpha_1 + \alpha_2] + \alpha_3 h_\tau = 0, \tag{4.39}$$

with $h_\tau \propto \exp(\delta\tau)$, has eigenvalues

$$\delta = \left[-[\tilde{k}^{-1}\alpha_1 + \alpha_2] \pm \sqrt{[\tilde{k}^{-1}\alpha_1 + \alpha_2]^2 - 4\alpha_0 \tilde{k}^{-1} \alpha_3} \right] \Big/ 2\alpha_0. \tag{4.40}$$

For $1.2 \leqslant \gamma \leqslant 1.6$ and $1 \leqslant Q \leqslant 8$, eigenvalues are imaginary, stable for $\tilde{k}^{-1}\alpha_1 + \alpha_2 < 0$, unstable for $\tilde{k}^{-1}\alpha_1 + \alpha_2 > 0$ and neutrally stable for $\tilde{k}^{-1}\alpha_1 + \alpha_2 = 0$. Note that the location of the neutral stability is not a function of the activation energy in the induction zone, to the order calculated. This is due to the dominance of the detonation structure by the zero-activation-energy recombination zone. Equation (4.37) can also be re-written in a phase-plane form with $u = h_\tau$ as

$$\left.\begin{aligned} \dot{u} &= v, \\ \dot{v} &= -[v[\tilde{k}^{-1}\alpha_1 + \alpha_2 \mathrm{e}^{-k_T u}] + \alpha_3 u + \alpha_4 \tilde{k}^{-1} v^2 \mathrm{e}^{-k_T u}] \tilde{k} \alpha_0^{-1} \mathrm{e}^{k_T u}, \end{aligned}\right\} \tag{4.41}$$

showing the presence of a single critical point $u = v = 0$.

5. Results

Figure 2(*a*) shows the neutral stability boundary obtained from the linear equation (4.40) with $\tilde{k} = 1$ for varying Q and γ. The system is stable to the left of the boundary, unstable to the right. For γ fixed, unstable regions are accessible for increasing Q, i.e. for more exothermic reactions, while for Q fixed, unstable regions are accessible for increasing γ, i.e where gas dynamic pressure fluctuations play an increasingly important role in determining a given temperature change. The frequency of the neutrally stable mode is shown in figure 2(*b*). The change in growth rate and frequency of the linear modes (4.40) is shown in figure 3 for varying Q and three values of γ. Each mode undergoes a Hopf bifurcation in passing from stable to unstable regions.

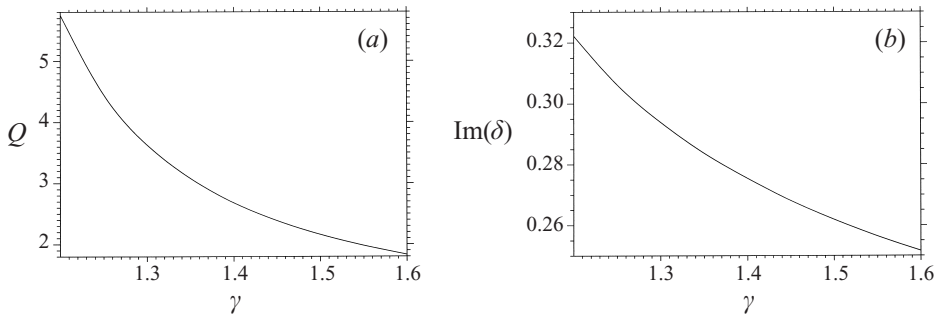

FIGURE 2. (*a*) Neutral stability curve for $\tilde{k} = 1$ with varying Q and γ. (*b*) Disturbance frequency along the neutral stability curve.

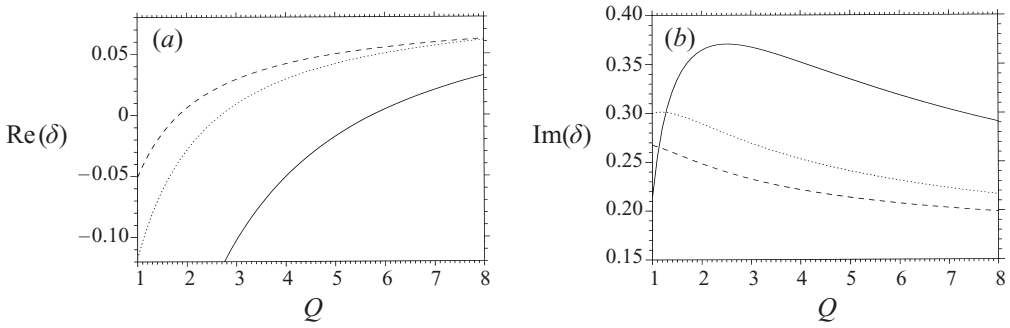

FIGURE 3. (*a*) Growth rate and (*b*) frequency verses Q for $\tilde{k} = 1$ and $\gamma = 1.2$ (solid line), $\gamma = 1.4$ (dotted line) and $\gamma = 1.6$ (dashed line).

The corresponding nonlinear behaviour is obtained by solving numerically the evolution equation (4.37) using standard fourth-order Runge–Kutta algorithms. The initial conditions in all the cases shown below are $h_\tau = 0$, $h_{\tau\tau} = 0.01$. Figure 4(*a*) shows the evolution of the shock velocity perturbation when $Q = 1.5$, $\gamma = 1.6$ and $\tilde{k} = 1$ ($\alpha_1/\alpha_0 = 0.219$, $\alpha_2/\alpha_0 = -0.189$, $\alpha_3/\alpha_0 = 0.067$, and $\alpha_4/\alpha_0 = -k_T = 0.856$), where $\mathrm{Re}\,(\delta) = -0.148$ and $\mathrm{Im}\,(\delta) = 0.258$ (period 24.3). As expected, the solution decays from its initial perturbation to the equilibrium point $h_\tau = h_{\tau\tau} = 0$. The corresponding phase portrait of the decay is shown in figure 4(*b*). Figure 5 shows the evolution when $Q = 2$, $\gamma = 1.6$ and $\tilde{k} = 1$ where $\mathrm{Re}\,(\delta) = 0.00612$ and $\mathrm{Im}\,(\delta) = 0.2484$ (period 25.29), i.e. when the linear system is unstable. There is a slow growth of the shock velocity perturbation until it limits to a stable periodic limit-cycle solution with period 25.5 and amplitude 1.717. Increasing Q leads to increasingly unstable solutions. Figure 6 shows the evolution for $Q = 2.5$, $\gamma = 1.6$ and $\tilde{k} = 1$ ($\alpha_1/\alpha_0 = 0.162$, $\alpha_2/\alpha_0 = -0.202$, $\alpha_3/\alpha_0 = 0.058$, and $\alpha_4/\alpha_0 = -k_T = 0.896$), where $\mathrm{Re}\,(\delta) = 0.01979$, $\mathrm{Im} = 0.2399$ (period 26.2). The long time solution is again a stable periodic limit cycle having period 26.7 and amplitude 3.7. Note the increased amplitudes of the acceleration and deceleration during the growth and decay phases of the cycle, as seen in the phase portraits as Q increases from $Q = 2$ to $Q = 2.5$.

Figures 7, 8 and 9 show the resulting evolution obtained by further increases in Q, specifically $Q = 3$, $Q = 3.5$ and $Q = 4$ respectively for $\gamma = 1.6$ and $\tilde{k} = 1$. For $Q = 4$, $\alpha_1/\alpha_0 = 0.127$, $\alpha_2/\alpha_0 = -0.211$, $\alpha_3/\alpha_0 = 0.051$, and $\alpha_4/\alpha_0 = -k_T = 0.935$. The trend is that all evolutions approach a stable periodic limit cycle with periods 28.5, 30.6 and 33.1, corresponding to periods of the linear modes 27.0, 27.7 and 28.4, but that the

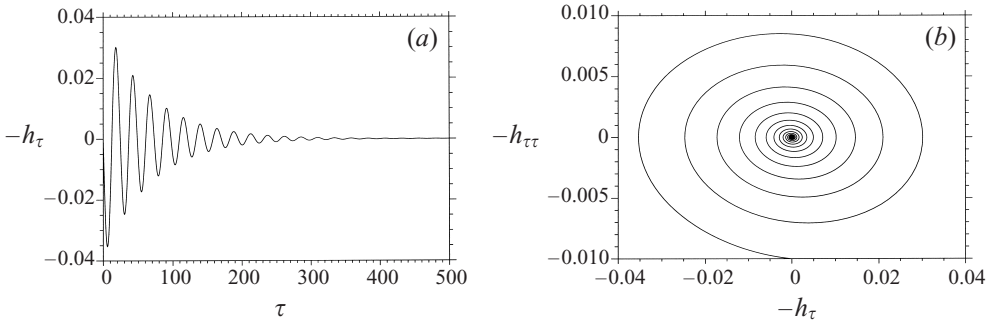

FIGURE 4. (*a*) Evolution of the shock velocity perturbation h_τ for $Q = 1.5$, $\gamma = 1.6$ and $\tilde{k} = 1$. (*b*) Corresponding phase portrait.

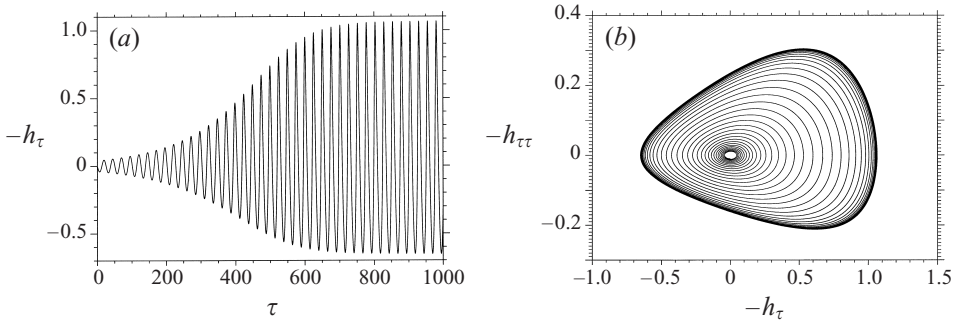

FIGURE 5. As figure 4 but for $Q = 2$.

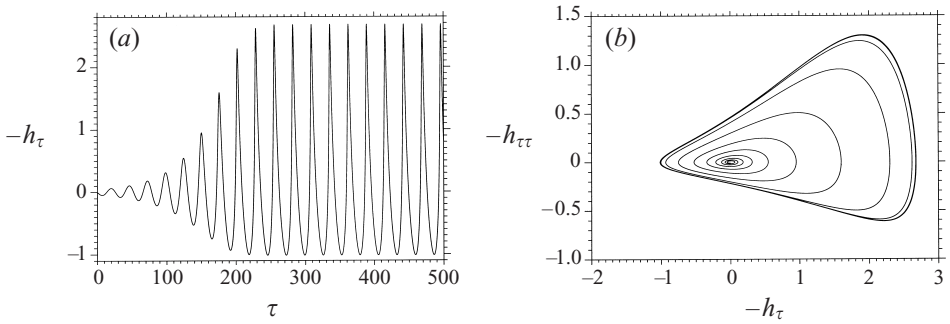

FIGURE 6. As figure 4 but for $Q = 2.5$.

amplitude of the limit cycles, namely 5.7, 8.3, 11.25, increases. There is, however, a marked change in the behaviour of the phase portrait for increasing Q. In figure 9, there is a fast stage during the growth phase of the cycle associated with a large magnitude of acceleration, a rapid deceleration around the peak of the cycle, and a slow decay stage of the cycle involving much lower magnitudes of deceleration. The non-symmetric nature of the cycle, involving fast acceleration and slow deceleration phases, is also observed in the direct numerical calculations of Short & Quirk (1997) as the amplitude of the limit cycle increases, i.e. as T_B increases.

In all calculations performed, we have found that the limiting behaviour is a stable limit cycle, with the amplitude of the cycle growing as regions of greater instability are

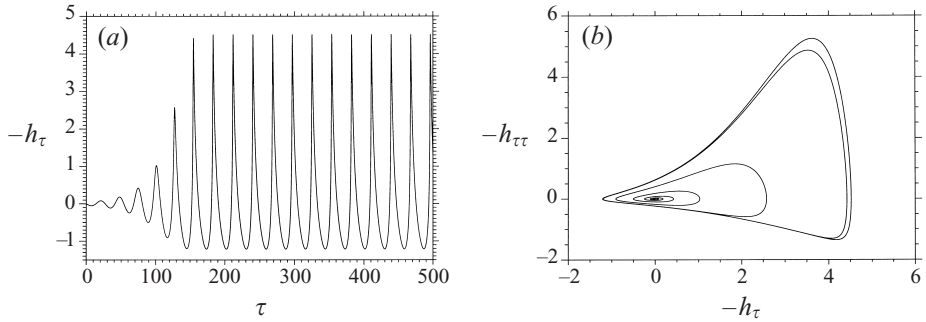

FIGURE 7. As figure 4 but for $Q = 3$.

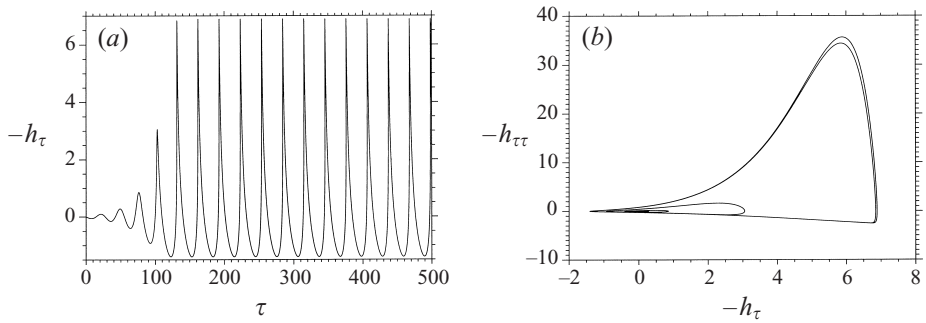

FIGURE 8. As figure 4 but for $Q = 3.5$.

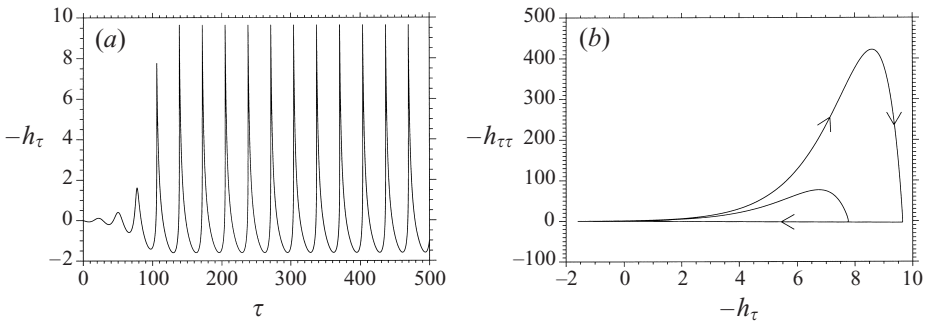

FIGURE 9. As figure 4 but for $Q = 4$.

encountered, a behaviour apparently different from the evolution equation derived by Yao & Stewart (1996) for a one-step reaction. In their case, in addition to stable periodic limit cycles, there are regions of singular unbounded growth in the shock velocity perturbation, particularly as $\theta \to \infty$, where the Yao–Stewart equation limits to that previously derived by Buckmaster (1988). Also of note is the similarity in period of the linearly unstable mode compared with the period of the corresponding nonlinear periodic limit cycle, a feature widely recognized in pulsating detonations for both one-step and three-step reactions (Bourlioux *et al.* 1991; Quirk 1994; Short & Quirk 1997; Sharpe & Falle 1999). This would indicate that the physical mechanisms which govern the nonlinear stability of pulsating detonations appear to be captured well by the linear oscillator (4.39).

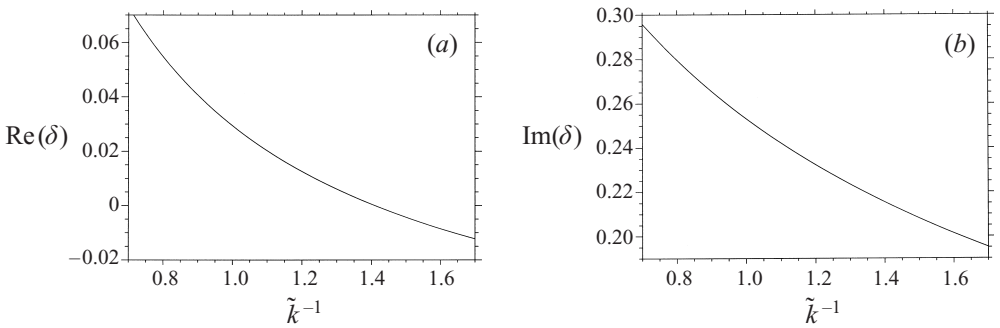

FIGURE 10. (*a*) Growth rate and (*b*) frequency versus $\tilde{k}^{-1}$ for $Q = 4$ and $\gamma = 1.4$.

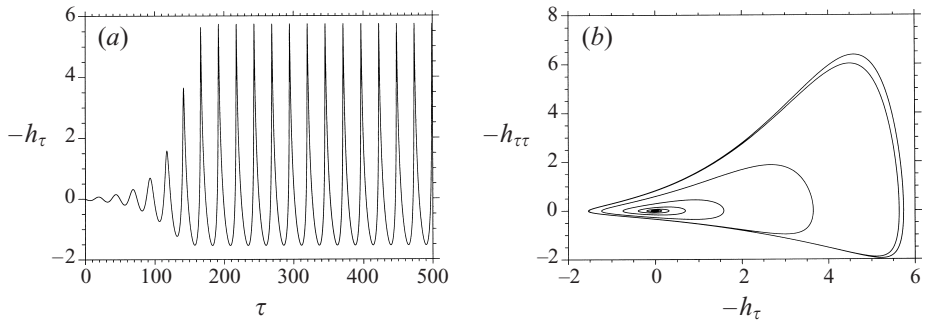

FIGURE 11. (*a*) Evolution of the shock velocity perturbation h_τ for $Q = 4$, $\gamma = 1.4$ and $\tilde{k}^{-1} = 1$. (*b*) Corresponding phase portrait.

The transient fast and slow nature of the phase portraits, found above, also raises concerns about resolution in the current state-of-the-art direct numerical calculations of pulsating detonations, (Bourlioux *et al.* 1991; Quirk 1994; Short & Quirk 1997; Sharpe & Falle 1999), where the resolution required to resolve such transient solutions is far greater than any direct numerical calculations of pulsating detonations that have been performed to date. Since the present evolution equation apparently predicts stable, but large-amplitude, periodic solutions in all cases (although we have been unable to rule out the presence of unstable periodic solutions purely based on the form of the evolution equation), it would be worthwhile to re-examine the findings of period-doubling and chaotic propagating detonations in numerical studies under much higher resolution.

The final set of calculations examine the behaviour for increasing $\tilde{k}^{-1}$, corresponding to a widening of the chain-termination region. This refers directly to the study by Short & Quirk (1997), where the effects of varying the length of the chain-termination region relative to the chain-induction zone, controlled by the chain-branching temperature T_B, were examined. Stable solutions were predicted for lower T_B, or in the limit of a widening chain-termination region relative to the chain-induction zone. In the present study, decreasing $\tilde{k}$ corresponds to decreasing the reaction rate (3.3), and longer chain-termination regions. Figure 10 shows the evolution of the growth rate and frequency with $\tilde{k}^{-1}$ for the linear mode (4.40) for $Q = 4$ and $\gamma = 1.4$. As $\tilde{k}^{-1}$ increases, the stable modes are encountered, as expected. Figures 11, 12 and 13 show the nonlinear evolution corresponding to $\tilde{k}^{-1} = 1$, $\tilde{k}^{-1} = 1.2$, and $\tilde{k}^{-1} = 1.6$ respectively. For $\tilde{k}^{-1} = 1$, $\mathrm{Re}(\delta) = 0.0294$ and $\mathrm{Im}(\delta) = 0.253$ (period 24.84) and

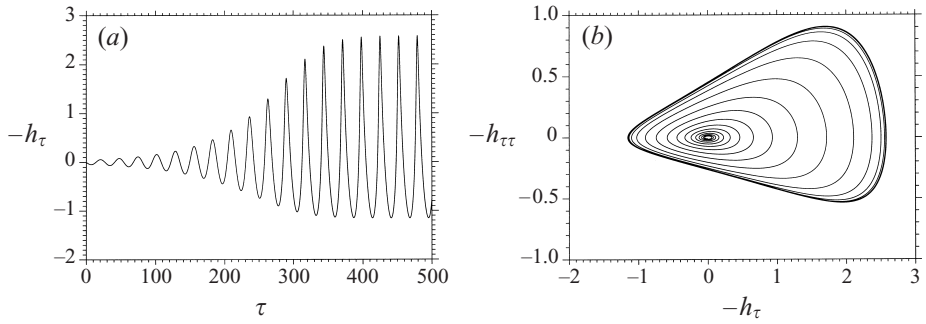

FIGURE 12. As figure 11 but for $\tilde{k}^{-1} = 1.2$.

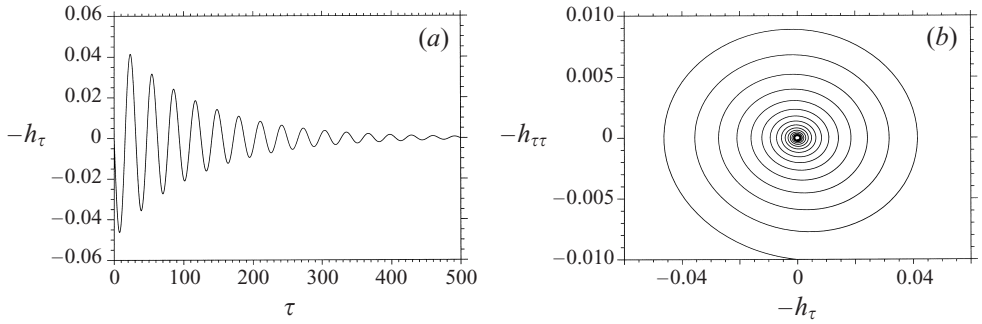

FIGURE 13. As figure 11 but for $\tilde{k}^{-1} = 1.6$.

the unstable growth limits to a periodic solution of amplitude 7.3 and period 25.55. Similarly in figure 12, $\tilde{k}^{-1} = 1.2$ ($\alpha_1/\alpha_0 = 0.144$, $\alpha_2/\alpha_0 = -0.203$, $\alpha_3/\alpha_0 = 0.065$, and $\alpha_4/\alpha_0 = -k_T = 0.696$) with $\mathrm{Re}(\delta) = 0.0126$ and $\mathrm{Im}(\delta) = 0.232$ (period 27.08), and the resulting evolution is a limit cycle of period 27.0 and amplitude 3.725. For $\tilde{k}^{-1} = 1.6$, $\mathrm{Re}(\delta) = -0.0085$ and $\mathrm{Im}(\delta) = 0.2014$, and the initial perturbation decays to the equilibrium solution $h_\tau = h_{\tau\tau} = 0$. Short & Quirk (1997) found that stable detonations are found for temperature-independent chain-termination regions longer than temperature-dependent chain-induction regions, a trend mimicked by our evolution equation (4.37).

6. Summary

A nonlinear evolution equation for pulsating Chapman–Jouguet detonations with chain-branching kinetics has been derived. We consider a model reaction system having two components: a thermally neutral chain-branching induction zone governed by an Arrhenius reaction, terminating at a location where conversion of fuel into chain radical occurs; and a longer exothermic main reaction layer or chain-recombination zone having a temperature-independent reaction rate. The evolution equation is autonomous and second-order in time in the shock velocity perturbation. It predicts unstable solutions for increasing exothermicity, for increasing specific heats ratio, and decreasing ratio of the length of the chain-recombination zone to chain-induction zone. In all cases calculated, unstable solutions lead to stable periodic limit cycles. These dynamics correspond remarkably well with numerical solutions conducted earlier for a model three-step chain-branching reaction.

The author would like to thank Dr J. B. Bdzil and Professor J. D. Buckmaster for useful discussions, and Dr Joe Foster at Eglin A. F. B. for financial support for a visit in June 1998 where this project began. The work was funded by the Air Force Office of Scientific Research (Dr Arje Nachman, sponsor).

Appendix. Formulae

The coefficients appearing in the shock relations (4.5) are given by

$$\left.\begin{aligned} k_u &= \frac{(\mu-1)}{\mu(M_s^2-1)}[-1-(1-(\gamma-1)(\mu-1))M_s^2], \\ k_p &= \frac{(\mu-1)M_s}{\mu(M_s^2-1)}[2-(\gamma-1)(\mu-1)M_s^2], \\ k_T &= (\gamma-1)\frac{(\mu-1)M_s}{\mu(M_s^2-1)}[2+(\mu-1)(1-\gamma M_s^2)], \\ k_\rho &= \frac{(\mu-1)M_s}{\mu(M_s^2-1)}[2-(\gamma-1)(\mu-1)], \end{aligned}\right\} \tag{A 1}$$

where

$$\mu = \frac{(\gamma+1)D^2}{2+(\gamma-1)D^2} \tag{A 2}$$

is the ratio of the shocked gas density to the unperturbed pre-shock gas density. The formulae A_1 and A_2 appearing in the compatibility relation (4.29) are given by

$$\begin{aligned} A_1 = u^{(0)}|_{\lambda=1}\frac{(\gamma+1)}{(\gamma-1)}[M_s k_\rho + k_u - 1] + \frac{2\gamma M_s}{(\gamma-1)} \\ +\rho^{(0)}|_{\lambda=1}\left[\frac{1}{(\gamma-1)}(\gamma k_p - k_\rho) + M_s(k_u-1)\right], \end{aligned} \tag{A 3}$$

and

$$A_2 = -u^{(0)}|_{\lambda=1}\frac{(\gamma+1)}{(\gamma-1)} + \frac{2\gamma M_s}{(\gamma-1)} - M_s\rho^{(0)}|_{\lambda=1}. \tag{A 4}$$

The formulae B_1 and B_2 appearing in the $O(\epsilon)$ density perturbation $\rho^{(1)}$ (4.28) are given by

$$\left.\begin{aligned} B_1 &= \frac{(\gamma-1)}{\eta}[(A_3(u^{(0)}-u^{(0)}|_{\lambda=1}) + A_4(\rho^{(0)}-\rho^{(0)}|_{\lambda=1})], \\ B_2 &= \frac{(\gamma-1)}{\eta}[(A_5(u^{(0)}-u^{(0)}|_{\lambda=1}) + A_6(\rho^{(0)}-\rho^{(0)}|_{\lambda=1})], \end{aligned}\right\} \tag{A 5}$$

where

$$\left.\begin{aligned} A_3 = \frac{(\gamma+1)}{(\gamma-1)}[M_s k_\rho + k_u - 1], \quad A_4 = \frac{1}{(\gamma-1)}(\gamma k_p - k_\rho) + M_s(k_u-1), \\ A_5 = -\frac{(\gamma+1)}{(\gamma-1)}, \quad A_6 = -M_s. \end{aligned}\right\} \tag{A 6}$$

The formulae B_3 and B_4 appearing in the $O(\epsilon)$ velocity perturbation $u^{(1)}$ (4.28) are given by

$$\left.\begin{aligned} B_3 &= \frac{(\gamma-1)}{\eta}\left[A_7\left(\frac{1}{[\rho^{(0)}]^2}-\frac{1}{[\rho^{(0)}]^2_{\lambda=1}}\right)+A_8\left(\frac{1}{\rho^{(0)}}-\frac{1}{\rho^{(0)}|_{\lambda=1}}\right)\right.\\ &\quad \left.+A_{10}(u^{(0)}-u^{(0)}|_{\lambda=1})+A_{11}([u^{(0)}]^2-[u^{(0)}]^2_{\lambda=1})\right],\\ B_4 &= \frac{(\gamma-1)}{\eta}\left[A_{12}\left(\frac{1}{[\rho^{(0)}]^2}-\frac{1}{[\rho^{(0)}]^2_{\lambda=1}}\right)+A_{13}\left(\frac{1}{\rho^{(0)}}-\frac{1}{\rho^{(0)}|_{\lambda=1}}\right)\right.\\ &\quad \left.+A_{14}(u^{(0)}-u^{(0)}|_{\lambda=1})+A_{11}([u^{(0)}]^2-[u^{(0)}]^2_{\lambda=1})\right], \end{aligned}\right\} \tag{A 7}$$

where

$$\left.\begin{aligned} A_7 &= -\frac{\gamma}{(\gamma-1)}[M_s k_\rho + k_u - 1]\left(\frac{1}{\gamma}+M_s^2\right), \quad A_8 = -\frac{\gamma}{(\gamma-1)}\left[\frac{1}{\gamma}+M_s^2\right],\\ A_{10} &= -\left[\frac{1}{(\gamma-1)}(\gamma k_p - k_\rho)+M_s(k_u-1)\right], \quad A_{11} = -1,\\ A_{12} &= \frac{\gamma}{(\gamma-1)}\left[\frac{1}{\gamma}+M_s^2\right], \quad A_{13} = -A_{12}, \quad A_{14} = -A_6. \end{aligned}\right\} \tag{A 8}$$

The formulae B_5 and B_6 appearing in the $O(\epsilon)$ pressure perturbation $p^{(1)}$ (4.28) are given by

$$\begin{aligned} B_5 &= \frac{(\gamma-1)}{\eta}\left[A_{15}\left[u^{(0)}\left([u^{(0)}]^2+\frac{2\gamma}{(\gamma-1)}\frac{p^{(0)}}{\rho^{(0)}}\right)-u^{(0)}|_{\lambda=1}\left([u^{(0)}]^2+\frac{2\gamma}{(\gamma-1)}\frac{p^{(0)}}{\rho^{(0)}}\right)_{\lambda=1}\right]\right.\\ &\quad +A_{16}\left[\left([u^{(0)}]^2+\frac{2\gamma}{(\gamma-1)}\frac{p^{(0)}}{\rho^{(0)}}\right)-\left([u^{(0)}]^2+\frac{2\gamma}{(\gamma-1)}\frac{p^{(0)}}{\rho^{(0)}}\right)_{\lambda=1}\right]\\ &\quad \left.+A_{18}[u^{(0)}-u^{(0)}|_{\lambda=1}]+A_{19}([u^{(0)}]^2-[u^{(0)}]^2_{\lambda=1})\right], \end{aligned} \tag{A 9}$$

$$\begin{aligned} B_6 &= \frac{(\gamma-1)}{\eta}\left[A_{11}\left[u^{(0)}\left([u^{(0)}]^2+\frac{2\gamma}{(\gamma-1)}\frac{p^{(0)}}{\rho^{(0)}}\right)-u^{(0)}|_{\lambda=1}\left([u^{(0)}]^2+\frac{2\gamma}{(\gamma-1)}\frac{p^{(0)}}{\rho^{(0)}}\right)_{\lambda=1}\right]\right.\\ &\quad +A_{14}\left[\left([u^{(0)}]^2+\frac{2\gamma}{(\gamma-1)}\frac{p^{(0)}}{\rho^{(0)}}\right)-\left([u^{(0)}]^2+\frac{2\gamma}{(\gamma-1)}\frac{p^{(0)}}{\rho^{(0)}}\right)_{\lambda=1}\right]\\ &\quad \left.+A_{20}[u^{(0)}-u^{(0)}|_{\lambda=1}]+A_{14}([u^{(0)}]^2-[u^{(0)}]^2_{\lambda=1})\right], \end{aligned} \tag{A 10}$$

where

$$\left.\begin{aligned} A_{15} &= M_s k_\rho + k_u - 1, \quad A_{16} = -A_6, \quad A_{19} = -A_6, \quad A_{20} = -M_s^2,\\ A_{18} &= M_s\left[\frac{1}{(\gamma-1)}(\gamma k_p - k_\rho)+M_s(k_u-1)\right]. \end{aligned}\right\} \tag{A 11}$$

The formulae B_7 and B_8 appearing in the $O(\epsilon)$ reaction progress perturbation $\lambda^{(1)}$ (4.35) are given by

$$B_7 = -(1-\lambda)^{1/2}\int_0^\lambda \frac{B_3-1}{u^{(0)}(1-\lambda)^{1/2}}\,\mathrm{d}\lambda, \quad B_8 = -(1-\lambda)^{1/2}\int_0^\lambda \frac{B_4-1}{u^{(0)}(1-\lambda)^{1/2}}\,\mathrm{d}\lambda. \tag{A 12}$$

Finally, the integrals I_1 to I_6 appearing in the evolution equation (4.37) and (4.38) are given by

$$\left.\begin{aligned}
I_1 &= -\int_0^\lambda \frac{u^{(0)}}{r^{(0)}} B_1 \,\mathrm{d}\lambda, \quad I_2 = -\int_0^\lambda \frac{u^{(0)}}{r^{(0)}} B_2 \,\mathrm{d}\lambda,\\
I_3 &= -\int_0^\lambda \frac{u^{(0)}}{r^{(0)}} \left[u^{(0)} B_1 + \rho^{(0)} B_3\right] \mathrm{d}\lambda,\\
I_4 &= -\int_0^\lambda \frac{u^{(0)}}{r^{(0)}} \left[u^{(0)} B_2 + \rho^{(0)} B_4\right] \mathrm{d}\lambda,\\
I_5 &= -\int_0^\lambda \frac{u^{(0)}}{r^{(0)}} B_3 + \frac{1}{r^{(0)}} \left[\frac{1}{(\gamma-1)\rho^{(0)}} B_5 - \frac{\gamma}{(\gamma-1)} \frac{p^{(0)}}{[\rho^{(0)}]^2} B_1 - \beta B_7\right] \mathrm{d}\lambda,\\
I_6 &= -\int_0^\lambda \frac{u^{(0)}}{r^{(0)}} B_4 + \frac{1}{r^{(0)}} \left[\frac{1}{(\gamma-1)\rho^{(0)}} B_6 - \frac{\gamma}{(\gamma-1)} \frac{p^{(0)}}{[\rho^{(0)}]^2} B_2 - \beta B_8\right] \mathrm{d}\lambda.
\end{aligned}\right\} \tag{A 13}$$

The Chapman–Jouguet detonation velocity D is given by

$$D = \left[\left(1 + \frac{(\gamma^2-1)}{\gamma} Q\right) + \left(\left(1 + \frac{(\gamma^2-1)}{\gamma} Q\right) - 1\right)^{1/2}\right]^{1/2}. \tag{A 14}$$

REFERENCES

Abouseif, G. & Toong, T. Y. 1982 Theory of unstable one-dimensional detonations. *Combust. Flame* **45**, 64–94.

Alpert, R. L. & Toong, T. Y. 1972 Periodicity in exothermic hypersonic flows about blunt projectiles. *Acta Astronaut.* **17**, 538–560.

Bourlioux, A., Majda, A. J. & Roytburd, V. 1991 Theoretical and numerical structure for unstable one-dimensional detonations. *SIAM J. Appl. Maths* **51**, 303–343.

Buckmaster, J. D. 1988 Pressure transients and the genesis of transverse shocks in unstable detonations. *Combust. Sci. Tech.* **61**, 1–20.

Buckmaster, J. D. & Ludford, G. S. S. 1982 *Theory of Laminar Flames.* Cambridge University Press.

Buckmaster, J. D. & Ludford, G. S. S. 1986 The effect of structure on the stability of detonations I. Role of the induction zone. In *Twenty-first Symp. (Intl) on Combustion*, pp. 1669–1676. The Combustion Institute.

Clavin, P. & He, L. T. 1996 Stability and nonlinear dynamics of one-dimensional overdriven detonations in gases. *J. Fluid Mech.* **306**, 353–378.

Fickett, W., Jacobson, J. D. & Schott, G. L. 1972 Calculated pulsating one-dimensional detonations with induction-zone kinetics. *AIAA J.* **10**, 514–516.

Kaneshige, M. J. & Shepherd, J. E. 1996 Oblique detonation stabilized on a hypervelocity projectile. In *26th Symp. (Intl) on Combustion*, p. 3015. The Combustion Institute.

Lehr, H. F. 1972 Experiments on shock-induced combustion. *Astronaut. Acta* **17**, 589–597.

McVey, J. B. & Toong, T. Y. 1971 Mechanism of instabilities of exothermic hypersonic blunt-body flows. *Combust. Sci. Tech.* **3**, 63–76.

Oran, E. S. & Boris, J. 1987 *Numerical Simulation of Reactive Flow*. Elsevier.

Quirk, J. J. 1994 Godunov-type schemes applied to detonation flows. In *Combustion in High-Speed Flows* (ed. J. Buckmaster, T. L. Jackson & A. Kumar), pp. 575–596. Kluwer.

Sharpe, G. J. & Falle, S. A. E. G. 1999 One-dimensional numerical simulations of idealized detonations. *Proc. R. Soc. Lond.* A **455**, 1203–1214.

Short, M. 1996 An asymptotic derivation of the linear stability of the square wave detonation using the Newtonian limit. *Proc. R. Soc. Lond.* A **452**, 2203–2224.

Short, M. 1997 A parabolic linear evolution equation for cellular detonation instability. *Combust. Theory Modell.* **1**, 313–346.

Short, M., Kapila, A. K. & Quirk, J. J. 1999 The chemical-gas dynamic mechanisms of pulsating detonation wave instability. *Phil. Trans. R. Soc. Lond.* A **357**, 3621–2638.

Short, M. & Quirk, J. J. 1997 On the nonlinear stability and detonability limit of a detonation wave for a model 3-step chain-branching reaction. *J. Fluid. Mech.* **339**, 89–119.

Short, M. & Stewart, D. S. 1997 Low-frequency two-dimensional linear instability of plane detonation. *J. Fluid Mech.* **340**, 249–295.

Short, M. & Stewart, D. S. 1999 Multi-dimensional stability of weak-heat-release detonations. *J. Fluid Mech.* **382**, 109–136.

Yao, J. & Stewart, D. S. 1996 On the dynamics of multi-dimensional detonation waves. *J. Fluid Mech.* **309**, 225–275.